



Polyamide thin-film composite membrane based on nano-silica modified polysulfone microporous support layer for forward osmosis

Yangbo Huang, Haiyang Jin, Ping Yu*, Yunbai Luo

College of Chemistry and Molecular Sciences, Wuhan University, Wuhan 430072, Hubei, People's Republic of China, Tel. +86 13659834359; email: bobo180899@whu.edu.cn (Y. Huang), Tel. +86 13667151729; email: haiyang@whu.edu.cn (H. Jin), Tel. +86 27 68752511; email: yuping@whu.edu.cn (P. Yu), Tel. +86 13807148090; email: ybai@whu.edu.cn (Y. Luo)

Received 23 April 2015; Accepted 11 October 2015

ABSTRACT

In this study, polyamide thin-film nanocomposite (TFN) membranes were prepared on nanosilica-modified polysulfone (PSf) support layers for forward osmosis (FO) applications. Different contents of SiO₂ nanoparticles (1, 3, and 5 wt%) were added to a dope solution to develop FO membranes with improved performance. The effects of SiO₂ on the membranes were investigated by attenuated total reflectance-Fourier transform infrared spectrometry, scanning electron microscope, hydrophilicity measurement, and mechanical property tests. The results showed that the wettability of PSf substrates was improved with increasing concentrations of SiO₂. The resulting TFN membranes had smaller structural parameters, which meant lower internal concentration polarization effects compared to typical thin-film composite membranes. However, SiO₂ nanoparticle is a good modifying agent to enhance water permeability, but it could not improve the selectivity of TFN membranes. The FO performance was evaluated using deionized water as feed solution and either 1 or 2 M NaCl as draw solution in both membrane orientations. The FO water flux of the fabricated membranes increased from 9.1 to 22.3 LMH when the active layer faced the feed solution (AL-FS) and 18.2 to 41.9 LMH when the active layer was placed towards the draw solution (AL-DS), mainly due to the improvement of PSf substrate with an addition of SiO₂.

Keywords: Forward osmosis; Thin-film nanocomposite membrane; Polysulfone; Polyamide; Silica nanoparticles

1. Introduction

As a novel membrane separation technology, forward osmosis (FO) has gained a growing popularity among many fields in recent years, such as seawater desalination [1–3], wastewater treatment [4,5], liquid food concentration [6,7], and power generation [8–10]. FO process utilizes osmotic pressure difference across the semipermeable membrane to force water from the

feed solution (FS) to the draw solution (DS). Pure water is then produced by separating the draw solute from the diluted DS. Compared to the external hydraulic pressure-driven membrane processes, FO potentially displays a higher water recovery and less membrane fouling [11–13].

However, the lack of an adequate membrane restricts the advance of FO technology in practical applications [14,15]. A promising FO membrane should show high water flux, low reverse salt

*Corresponding author.

diffusion, and good chemical resistance [14,16]. The current commercially available flat FO membrane made of cellulose triacetate (CTA) and the majority of thin-film composite (TFC) membranes [14,16,17] prepared in laboratory are asymmetric membranes with a dense skin layer and a porous support layer. One of the major obstacles in using these asymmetric membranes for FO processes is the presence of internal concentration polarization (ICP). ICP is an intrinsic phenomenon occurring inside the thick and hydrophobic porous support layer [18–20]. There are two types of ICP because of different membrane orientations. A dilutive ICP occurred when the active layer faces the feed solution (AL-FS), where the DS is diluted in the support layer. In the other case, a concentrative ICP happens as a result of accumulation of the solutes from the FS inside the porous support layer when the active layer is placed towards the draw solution (AL-DS) [16,21]. Osmotic pressure difference across the membrane reduces dramatically due to ICP, which is capable of causing a decrease in the water flux by more than 80% [18]. Since ICP happens inside the FO membrane, it cannot be eliminated by changing hydrodynamic conditions [1]. Therefore, one urgent task at present in FO research is to develop an appropriate membrane with a thin and hydrophilic substrate [15,22].

In the past years, hydrophilic modifications of polysulfone (PSf) membranes have been widely studied [17,23,24]. Young Hoon Cho et al. prepared a carboxylated polysulfone porous support membrane for FO processes [17]. They showed that the modified FO membranes had an observably higher water flux compared to the traditional polyamide thin-film composite (PA TFC) membranes. Other chemical modifications like sulfonation [25] and amination [26] also showed significantly enhanced hydrophilicity for the PSf membranes. Recently, researchers have mixed inorganic nanoparticles with the PSf dope solution to prepare a novel thin film nanocomposite (TFN) membrane [27–29]. These newly developed TFN membranes displayed a dramatic enhancement in water permeability.

Nanosilica has drawn particular attention because of its easy operation, mild reaction, well-known chemical properties, and fine suspendability with the polymer solution [21,29,30]. Previous researches have shown the potential of using SiO₂ nanoparticles as additive for the synthesis of ultrafiltration and pervaporation membranes with improved performance. As reported by Ahmad et al. [31], PSf ultrafiltration membrane modified by 5 wt% SiO₂ displayed 16 times higher water flux than that of unmodified membrane. The improved performance could owe to the enhanced hydrophilicity or increased membrane porosity.

In this work, TFN FO membranes were synthesized by incorporating hydrophilic SiO₂ nanoparticles into a polysulfone support layer. The membrane structure, intrinsic separation properties, and FO performance were analyzed to illuminate how SiO₂ nanoparticles could affect the water permeability of FO membranes.

2. Experimental materials and methods

2.1. Materials

Polysulfone beads (Mn: 75,000 Da, Solvay Advanced Polymers), 1-methyl-2-pyrrolidinone (NMP, ≥99.0%, Sinopharm Chemical Reagent Co., Ltd), and polyvinylpyrrolidone (PVP K-30, Sinopharm Chemical Reagent Co., Ltd) were used to prepare the substrates. Silica nanoparticles (20 nm, Sinopharm Chemical Reagent Co., Ltd) were blended with the dope solution to synthesize modified substrates. 1,3-phenylenediamine (MPD, ≥99.5%, Sinopharm Chemical Reagent Co., Ltd), trimesoyl chloride (TMC, ≥98.0%, Aladdin), and *n*-hexane (≥97.%, Sinopharm Chemical Reagent Co., Ltd) were used for interfacial polymerization. Sodium chloride (NaCl, ≥99.5%, Sinopharm Chemical Reagent Co., Ltd) was dissolved in deionized water (DI, 8–10 μs/cm) for FO and RO tests.

2.2. Preparation of PSf substrate

The PSf support membranes were prepared by phase inversion method [32]. According to Table 1, dope solutions were prepared by dissolving a certain percentage of PSf, PVP, and nano-SiO₂ particles in NMP and stirred by a mechanical stirrer (JJ, Yitong Electron Co., Ltd, China) at 70 °C for 8 h. Then the homogenous polymer solutions were placed in a desiccator at room temperature for 12–15 h to remove air bubbles. The dope solution was then spread on a dry glass plate using a casting knife at a gate height of 140 μm. The glass plate was immediately immersed into DI bath at room temperature to induce phase inversion. After the phase separation was finished, the substrate was peeled off and kept in DI bath before use.

2.3. Fabrication of polyamide active layer

The active layer of FO membrane was fabricated by interfacial polymerization on the surface of the prepared PSf substrate. At first, the substrate was soaked in 50 mL of 1% (w/v) aqueous solution of MPD for 120 s. The residual MPD solution on the surface of the substrate was removed using compressed nitrogen.

Table 1
Compositions of dope solutions for preparation of PSf substrate

Substrates	PSf (wt%)	NMP (wt%)	PVP (wt%)	SiO ₂ ^a (wt%)
PSf-0	14	85.5	0.5	0
PSf-1	14	85.5	0.5	1
PSf-3	14	85.5	0.5	3
PSf-5	14	85.5	0.5	5

^aThe mass of SiO₂ was based on the total mass of the dope solution.

Subsequently, 50 mL of 0.05% (w/v) TMC in the *n*-hexane solution was poured onto the membrane surface and held on the substrate for 120 s to form a polyamide film. The composite membrane was then rinsed thoroughly with DI water and stored in DI at room temperature before use. Four kinds of composite membranes were prepared in this work and named as TFC, TFN-1, TFN-3, and TFN-5 according to the compositions of PSf substrate, respectively.

2.4. Membrane characterizations

Attenuated total reflectance-Fourier transform infrared spectrometry (ATR-FTIR, Nicolet AVATAR 360) was used to identify the functional groups of the polyamide active layer and analyze the chemical changes of the PSf substrates. The cross-section and top surface morphologies of the membranes were observed under a FEI Quanta 200 scanning electron microscope (SEM, Holland) and a field-emission scanning electron microscope (FESEM, Sigma, Zeiss) from Germany. Energy dispersive spectrometry was used to confirm the presence of SiO₂. Based on the FESEM graphs, the size of pores on the membranes was measured using an ImageJ processing program.

Contact angle measurements were conducted by a DSA 100 instrument (KRÜSS GmbH, Germany) to indicate the wettability of the PSf substrates. The membrane porosity ε (%) was calculated by weighing the mass of wet and dry membrane samples [16,28].

$$\varepsilon = \frac{(m_w - m_d)/\rho_w}{(m_w - m_d)/\rho_w + m_d/\rho_p} \times 100\% \quad (1)$$

where m_w and m_d are the weights of wet and dry membrane samples, ρ_w and ρ_p are the densities of water and polymer, respectively.

Mechanical properties (e.g. tensile strength) of the membrane substrates were measured using an AGS-J tensile testing machine (Shimazu, Japan). Every membrane sample was dried under vacuum for 24 h before measurement.

2.5. Membrane performance test

Water permeability (A), salt permeability (B), and salt rejection (R) of the FO membranes were tested in a lab-scale cross-flow RO unit [33]. The effective membrane area (A_m) was 46.5 cm². The temperature of FS was maintained at 25 ± 0.5°C. External concentration polarization (ECP) was ignored due to a relatively high cross-flow velocity. Pure water flux (J_w) and water permeability were measured at an applied pressure of 2 bar and calculated using Eqs. (2) and (3):

$$J_w = \frac{\Delta V}{A_m \Delta t} \quad (2)$$

$$A = \frac{J_w}{\Delta P} \quad (3)$$

where ΔV is the volume of permeate water, Δt is the operating time, and ΔP is the applied pressure. Salt rejection and salt permeability were tested using 20 mM NaCl as FS at an operating pressure of 2 bar. The concentrations of FS (C_f) and permeate solution (C_p) were determined by an ICS-900 ion chromatography (Dionex, USA). R was evaluated by Eq. (4):

$$R = \left(1 - \frac{C_p}{C_f}\right) \times 100\% \quad (4)$$

Salt permeability was calculated by the measured values of A and R , and the known values of applied pressure ΔP , and osmotic pressure difference $\Delta\pi$:

$$\frac{1 - R}{R} = \frac{B}{A(\Delta P - \Delta\pi)} \quad (5)$$

The lab-scale cross-flow FO setup was similar to that reported in earlier literature [28]. In this work, the membrane cell had an effective area of 22.37 cm². Both draw and FSs were circulated in the closed loops at a cross-flow rate of 15.0 L/h by two diaphragm pumps (PLD-2203, China). NaCl solutions (1.0 and 2.0 M)

were used as DSs, while DI was used for FS. The temperature at which the FO performance tests were conducted was kept at $25 \pm 1^\circ\text{C}$. Both TFC and TFN membranes were tested in two membrane orientations: AL-DS and AL-FS.

The water flux, J_v , was measured by the weight increment in DS tank, which was placed on an electronic weighing balance. The FO setup was running for 10 min to stabilize water flux. Then weight increment data for 1 h were recorded and water flux was calculated using Eq. (6):

$$J_v = \frac{\Delta m_{\text{draw}}}{A_m \Delta t} \quad (6)$$

where Δm_{draw} is the mass change of DS and Δt is the measuring time.

The reverse salt flux, J_s , was determined by measuring the mass increment in NaCl in the FS at 1-h interval:

$$J_s = \frac{\Delta C_f V_f}{A_m \Delta t} \quad (7)$$

where ΔC_f is the concentration change in FS and V_f is referred to as the volume of FS. The concentration of the DS and the volume of the FS are hypothesized to be constant in the period of testing time. In order to minimize experimental error, each membrane was evaluated at least three times in both orientations.

The structural parameter, S , is closely related to FO performance and the average S value can be obtained experimentally using Eqs. (8) and (9), respectively [16,28,34]:

$$\text{AL-DS: } J_v = \frac{D}{S} \left[\ln \frac{A\pi_{\text{draw}} - J_v + B}{A\pi_{\text{feed}} + B} \right] \quad (8)$$

$$\text{AL-FS: } J_v = \frac{D}{S} \left[\ln \frac{A\pi_{\text{draw}} + B}{A\pi_{\text{feed}} + J_v + B} \right] \quad (9)$$

where D is the diffusion coefficient of the draw solute; π_{draw} and π_{feed} are the osmotic pressures of the DS and FS. S is also defined as follows:

$$S = \frac{l\tau}{\varepsilon} \quad (10)$$

where ε is the average porosity of the support layer, l is the membrane thickness, and τ is the tortuosity.

3. Results and discussion

3.1. Properties of PSf substrates with different contents of SiO_2 nanoparticles

Table 2 shows the properties of PSf membranes with different contents of SiO_2 nanoparticles. The modified substrates showed remarkably increased pure water fluxes compared to the original PSf membrane, because the presence of SiO_2 nanoparticles helped to enhance the wettability of the porous support layer which could effectively reduce the ICP effects during the FO process. The significant improvement of pure water flux was also due to the increased overall porosity and decreased structural parameters. In addition, the tensile strength of the membranes did not change much with the increase in the content of SiO_2 nanoparticles.

Fig. 1 shows the cross-section morphology of PSf substrates with different contents of SiO_2 nanoparticles. It shows that all the four types of PSf membranes display an asymmetric composite structure with a thin sponge-like layer on the top of a long finger-like layer. And the sponge-like layer was reported to be helpful to the fabrication of an integrated PA selective layer, while the long finger-like structure decreased mass transfer resistance [14]. Compared to the original PSf substrate (Fig. 1(a)), more long and thin finger-like micropores were found in the modified membranes. It is reported that the pore morphology is determined by the rate of polymer precipitation during the phase inversion process: fast precipitation generates finger-like pores and slow precipitation produces sponge-like pores [14]. Membranes with finger-like pore structure usually have higher porosity rather than that of sponge-like pores. So the changes occurring in the substrates may be due to the faster solvent–nonsolvent exchange rate during the process of phase inversion [28]. Thus, the dope solution with SiO_2 nanoparticles may precipitate rapidly, resulting in increased overall porosity [14,28]. An agglomeration phenomenon was observed when the concentration of SiO_2 was high (Fig. 1(c) and (d)) and some relatively large pores were produced nearby where SiO_2 agglomerated. This phenomenon demonstrated that interfacial tension existed at the organic–inorganic interface and the shrinking of polymer resulted in interfacial pores [31]. In addition, the precipitation of SiO_2 nanoparticles in the whole substrate preparation process may also lead to the inhomogeneous structure [35]. Moreover, the addition of SiO_2 in the casting solution increased the viscosity of the dope solution. The increased viscosity leads to a dense structure during the phase inversion process and resulted in a smaller pore size. Fig. 2

Table 2

Comparison of PSf substrates with different contents of SiO₂ nanoparticles

Substrates	Thickness (μm)	Pure water flux ^a (L/m ² h bar)	Contact angle ^b (°)	Porosity (%)	Tensile strength (MPa)	Structural parameter, S ^c (mm)
PSf-0	88 ± 3	526 ± 21	74.4 ± 2.0	57.0	7.96	0.90
PSf-1	86 ± 3	832 ± 7	71.1 ± 1.6	61.5	8.07	0.68
PSf-3	88 ± 4	1,071 ± 11	68.6 ± 0.9	63.1	7.98	0.55
PSf-5	85 ± 5	1,268 ± 42	66.4 ± 1.3	67.3	8.01	0.41

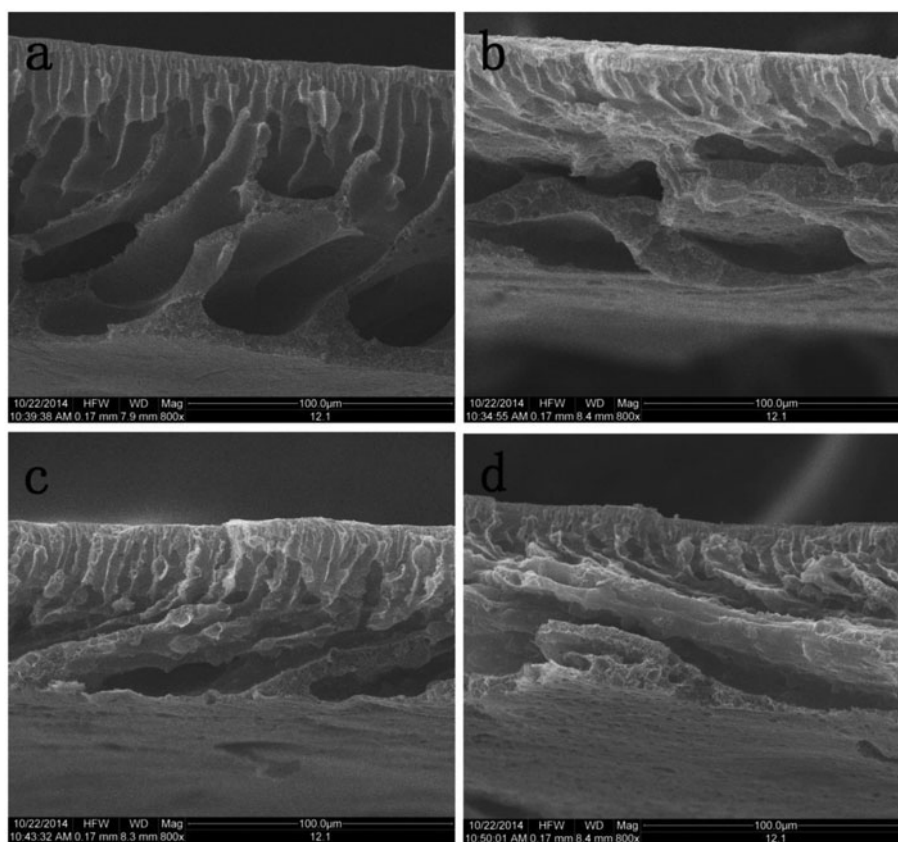
^aThe applied pressure was 2 bar.^bContact angle was measured at the top surface of substrates.^cThe average S value was experimentally determined from FO results using Eqs. (8) and (9).

Fig. 1. SEM micrographs of the cross section of PSf substrates (a) PSf-0, (b) PSf-1, (c) PSf-3, and (d) PSf-5.

shows the top surface morphology of the substrates. It is clear that the substrate surface is relatively flat and smooth, and many small pores can be observed. And with the increase in the SiO₂ nanoparticles, the size of pores on the membrane surface became smaller and smaller. This was further proved by the pore size distribution measurement. Fig. 3 shows that the mean pore size of the substrates shifted from bigger pores to small pores with the SiO₂ content increasing from 0 to 5%. Although the pore size of the TFN membranes decreased, the increased wettability and porosity

overrode the negative effect, contributing to better performance. Therefore, the results indicated that SiO₂ nanoparticles have a great influence on membrane morphology.

3.2. Effect of SiO₂ nanoparticles on the properties of composite membranes

Fig. 4 presents the ATR-FTIR spectra of TFC membrane and PSf substrates with different contents of

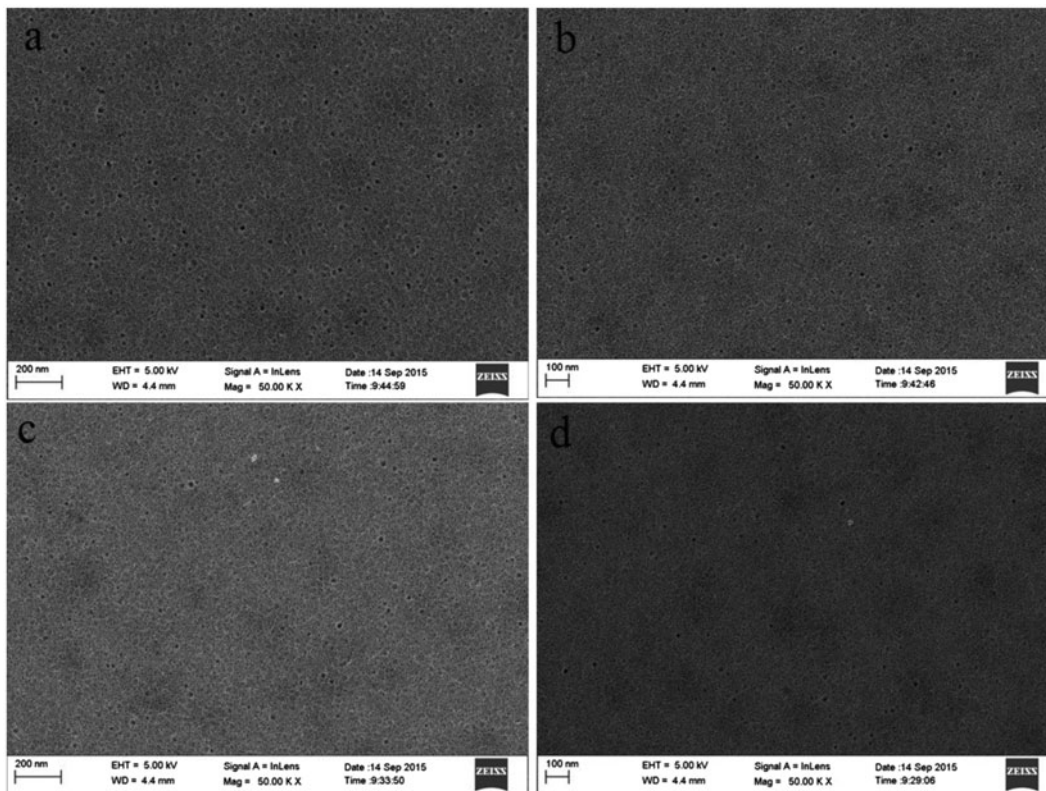


Fig. 2. SEM images of top surfaces of (a) PSf-0, (b) PSf-1, (c) PSf-3 and (d) PSf-5.

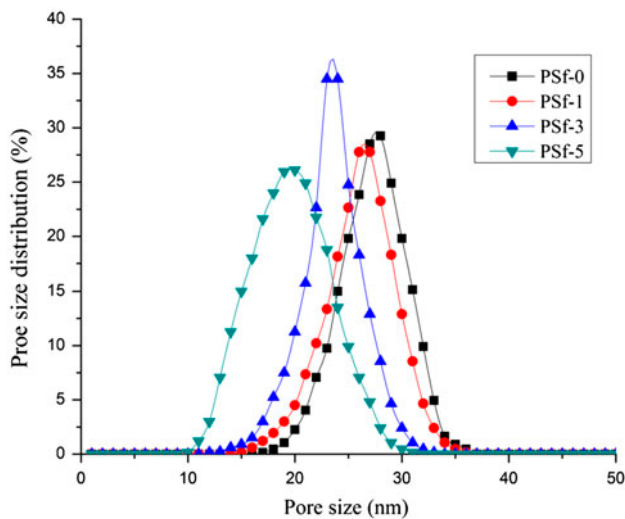


Fig. 3. Pore size distribution of original and modified PSf substrates.

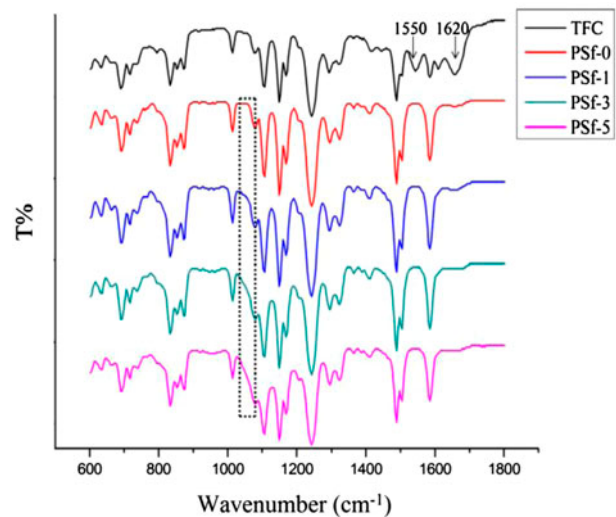


Fig. 4. ATR-FTIR spectra of TFC membrane and PSf substrates.

SiO₂ nanoparticles fabricated in this work. The characteristic peaks appeared at 1,540 and 1,625 cm⁻¹ were caused by the stretching of C–N and C=O in amide bands, respectively. This confirmed that the PA

layer had been successfully prepared on the surface of PSf substrate. The characteristic peaks of polysulfone were observed at 1,140 cm⁻¹ (asymmetric stretching of O=S=O), 1,160 cm⁻¹ (symmetric stretching of O=S=O),

1,245 cm^{-1} (asymmetric stretching of C–O–C), 1,500 cm^{-1} ($\text{CH}_3\text{–C–CH}_3$ stretching), and 1,400 cm^{-1} (benzene ring stretching). The peaks between 1,020–1,080 cm^{-1} gradually became stronger with the increase in the SiO_2 concentration. These changes may be due to the peak overlapping of a group on PSf and Si–O–Si [29]. However, no other significant difference was observed in the ATR-FTIR spectra of the modified PSf substrates. It is speculated that the dispersion of SiO_2 nanoparticles into the substrate is mainly due to the physical interactions [28]. The existence of SiO_2 particles in the modified membranes could be further confirmed by the EDX result shown in Fig. 5.

The top surface morphology of the composite membranes is shown in Fig. 6. The polyamide layer displayed a ridge and valley structure, which is typical of polyamide membranes formed via interfacial polymerization [14,16]. Fig. 6 shows that the polyamide layers of the four membranes are dense and continuous. The integrated PA layer indicates that the agglomerate of SiO_2 particles (shown in Fig. 1S) do not cause serious defects on the active layer. Theoretically, if there were defects on the surface of TFN membranes, the separation performance of these membranes will decrease sharply. According to Table 3, the salt rejection of the TFN membranes decreased from 86.18% (TFN-1) to 78.34% (TFN-5).

Table 3 shows the separation properties of membranes prepared in this work and commercial membranes. The synthesized FO membranes showed high water permeability and good NaCl rejection compared to some of the commercial FO membranes [16,21]. Water permeability increased from 2.69×10^{-12} m/s Pa for TFC to 3.36×10^{-12} m/s Pa for TFN-5, while salt permeability increased terribly from 3.95×10^{-8} m/s for TFC to 10.13×10^{-8} m/s for TFN-5. These results indicated a trade-off relationship between water permeability and salt permeability which was elucidated by

the previous study [11,36]. The increased water permeability was mainly attributed to the improvement of substrate wettability as well as the increased overall porosity and decreased structural parameters of the substrates. The B/A values of the synthesized membranes and some commercial membranes are also listed in Table 3. As discussed by Tang's group [16,37], the B/A value is directly related to the separation properties of an FO membrane. A larger B/A ratio can cause higher reverse salt flux, which may lead to a serious ICP due to the accumulation of salt inside the support layer. On the contrary, a smaller B/A ratio means lower salt diffusion from the DS to the FS as well as lower membrane fouling. In this study, the B/A ratio was increased with the addition of SiO_2 nanoparticles. The results show that although SiO_2 nanoparticle is a good modifying agent to enhance water permeability, it could not improve the selectivity of TFN membranes.

3.3. Effect of SiO_2 nanoparticles on the FO performance of the membranes

The FO performance of TFC and TFN membranes is shown in Figs. 7 and 8. Water flux and solute flux were tested using DI water as FS and either 1 or 2 M NaCl as DS under two membrane orientations: AL-DS and AL-FS. Fig. 7 shows that the FO water flux of the membranes increased from 9.1 to 22.3 LMH in AL-FS and 18.2 to 41.9 LMH in AL-DS as the content of SiO_2 nanoparticles in dope solution increased from 0 to 5 wt%. This could be due to the improved wettability and the decreased structural parameters of the SiO_2 -modified substrates. The results indicated that the existence of SiO_2 nanoparticles could effectively minimize the ICP effect during the FO process. The results also showed that a higher water flux could be achieved using a more concentrated DS (i.e. 2 M

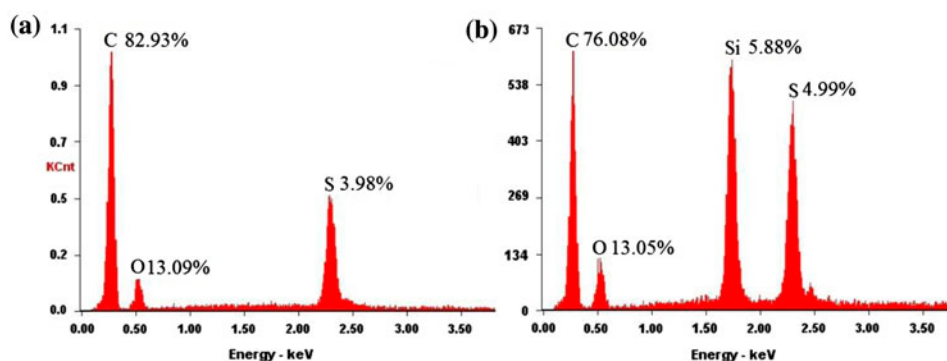


Fig. 5. EDX results of substrates (a) PSf-0 and (b) PSf-3.

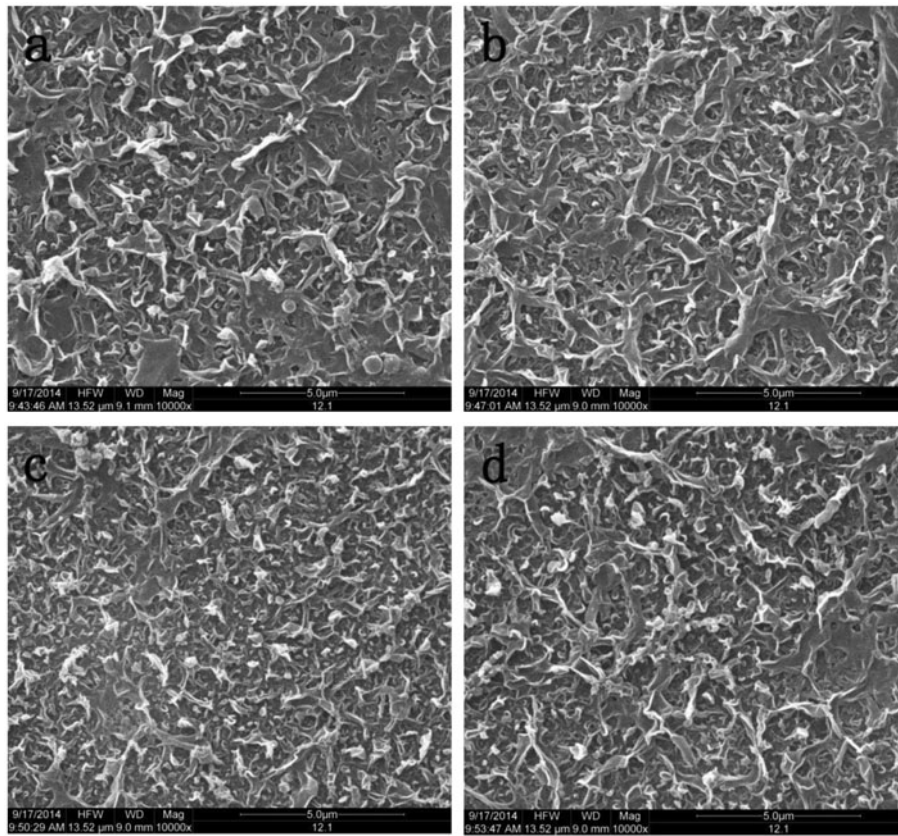


Fig. 6. SEM images of top surfaces of (a) TFC, (b) TFN-1, (c) TFN-3, and (d) TFN-5.

Table 3
Separation properties of membranes prepared in this work and commercial membranes

Membranes	Water permeability A ($\times 10^{-12}$ m/s Pa)	Salt permeability B ($\times 10^{-8}$ m/s)	NaCl rejection (%)	B/A (kPa)	Refs.
TFC	2.69	3.95	87.32	14.7	In this work
TFN-1	2.96	4.79	86.18	16.2	In this work
TFN-3	3.29	6.11	84.46	18.6	In this work
TFN-5	3.63	10.13	78.34	27.9	In this work
CTA-HW	3.3	25.6	78.5	84	[21]
CTA-W	0.9	4.0	81.9	47	[21]
CTA-NW	1.3	2.7	92.4	22	[21]
BW30	8.4	18.9	92.2	24	[16]
BW30-o	7.8	33.4	86.9	47	[16]

NaCl) as the water flux is closely related to the osmotic driving force provided by the DS.

Both Figs. 7 and 8 show that membrane orientation has a great influence on the performance of FO membranes. The AL-DS orientation showed a higher water

flux and solute flux than the AL-FS mode because there is no concentrative ICP effect when deionized water is used as FS in AL-DS mode. And the experiment results are consistent with most reports [21,28].

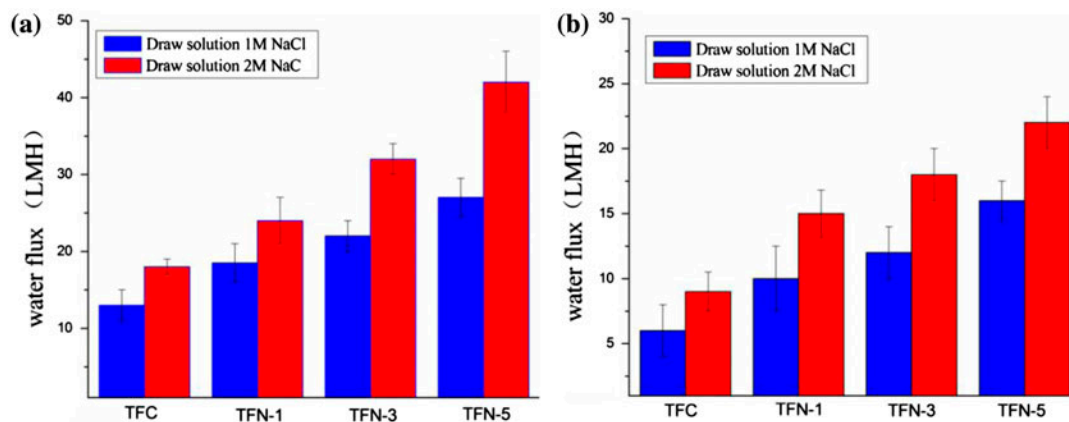


Fig. 7. Water fluxes of TFC and TFN membranes during FO process, (a) AL-DS orientation and (b) AL-FS orientation.

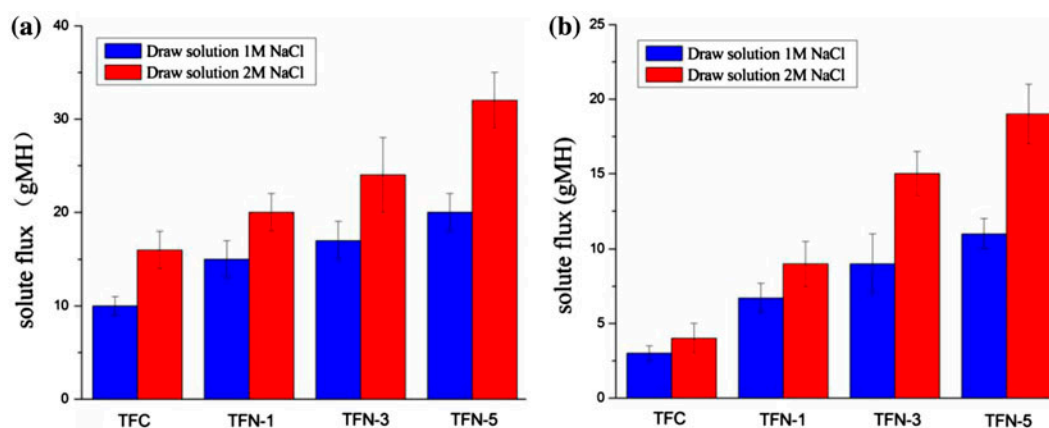


Fig. 8. Solute fluxes of TFC and TFN membranes during FO process, (a) AL-DS orientation and (b) AL-FS orientation.

Generally, an ideal FO membrane should have a high water flux and a low reverse salt flux. A high reverse salt flux can cause severe leakage of the draw solute. Fig. 8 shows the reverse salt flux of TFC and TFN membranes in both membrane orientations. The solute flux increased with an increasing concentration of SiO_2 nanoparticles. Although the desired water flux was achieved by TFN-5, the salt flux was as high as 32 ± 3 g of MH when tested in AL-DS orientation with 2 M NaCl as DS. The result was in accordance with the NaCl rejection data shown in Table 3. Therefore, excessive amounts of silica may have some negative impacts on the properties of FO membrane.

4. Conclusions

In this work, thin-film nanocomposite (TFN) membranes based on nanosilica-modified polysulfone microporous support layer were successfully synthe-

sized. Results showed that the addition of SiO_2 nanoparticles was able to enhance wettability, increase the overall porosity, and reduce the S value of the PSf substrate. The FO water flux of the fabricated membranes increased from 9.1 to 22.3 LMH in AL-FS and 18.2 to 41.9 LMH in AL-DS when 2 M NaCl was used as DS. However, a trade-off relationship between permeability and selectivity was found. SiO_2 nanoparticle is a good modifying agent to enhance water permeability, but it could not improve the selectivity of FO membranes. So it should be pointed out that excessive amounts of silica may have some negative impacts on the whole membrane properties.

Supplementary material

The supplementary material for this paper is available online at <http://dx.doi.org/10.1080/19443994.2015.1108874>.

Acknowledgment

This work was supported by the Plan of the National Science and Technology Support Program (2012BAC02B03).

References

- [1] S. Zhao, L. Zou, C.Y. Tang, D. Mulcahy, Recent developments in forward osmosis: Opportunities and challenges, *J. Membr. Sci.* 396 (2012) 1–21.
- [2] J.R. McCutcheon, R.L. McGinnis, M. Elimelech, Desalination by ammonia–carbon dioxide forward osmosis: Influence of draw and feed solution concentrations on process performance, *J. Membr. Sci.* 278 (2006) 114–123.
- [3] R.V. Linares, Z. Li, S. Sarp, S.S. Bucs, G. Amy, J.S. Vrouwenvelder, Forward osmosis niches in seawater desalination and wastewater reuse, *Water Res.* 66 (2014) 122–139.
- [4] A. Achilli, T.Y. Cath, E.A. Marchand, A.E. Childress, The forward osmosis membrane bioreactor: A low fouling alternative to MBR processes, *Desalination* 239 (2009) 10–21.
- [5] X. Zhang, Z. Ning, D.K. Wang, J.C.D. Costa, Processing municipal wastewaters by forward osmosis using CTA membrane, *J. Membr. Sci.* 468 (2014) 269–275.
- [6] B. Jiao, A. Cassano, E. Drioli, Recent advances on membrane processes for the concentration of fruit juices: A review, *J. Food Eng.* 63 (2004) 303–324.
- [7] E.M. Garcia-Castello, J.R. McCutcheon, M. Elimelech, Performance evaluation of sucrose concentration using forward osmosis, *J. Membr. Sci.* 338 (2009) 61–66.
- [8] A. Achilli, T.Y. Cath, A.E. Childress, Power generation with pressure retarded osmosis: An experimental and theoretical investigation, *J. Membr. Sci.* 343 (2009) 42–52.
- [9] A. Altaee, G. Zaragoza, A. Sharif, Pressure retarded osmosis for power generation and seawater desalination: Performance analysis, *Desalination* 344 (2014) 108–115.
- [10] E. Nagy, A general, resistance-in-series, salt- and water flux models for forward osmosis and pressure-retarded osmosis for energy generation, *J. Membr. Sci.* 460 (2014) 71–81.
- [11] X. Liu, H.Y. Ng, Double-blade casting technique for optimizing substrate membrane in thin-film composite forward osmosis membrane fabrication, *J. Membr. Sci.* 469 (2014) 112–126.
- [12] L.A. Hoover, W.A. Phillip, A. Tiraferri, N.Y. Yip, M. Elimelech, Forward with osmosis: Emerging applications for greater sustainability, *Environ. Sci. Technol.* 45 (2011) 9824–9830.
- [13] D.L. Shaffer, J.R. Werber, H. Jaramillo, S. Lin, M. Elimelech, Forward osmosis: Where are we now? *Desalination* 356 (2015) 271–284.
- [14] N.Y. Yip, A. Tiraferri, W.A. Phillip, J.D. Schiffman, M. Elimelech, High performance thin-film composite forward osmosis membrane, *Environ. Sci. Technol.* 44 (2010) 3812–3818.
- [15] D. Stillman, L. Krupp, Y.H. La, Mesh-reinforced thin film composite membranes for forward osmosis applications: The structure–performance relationship, *J. Membr. Sci.* 468 (2014) 308–316.
- [16] J. Wei, C. Qiu, C.Y. Tang, R. Wang, A.G. Fane, Synthesis and characterization of flat-sheet thin film composite forward osmosis membranes, *J. Membr. Sci.* 372 (2011) 292–302.
- [17] Y.H. Cho, J. Han, S. Han, M.D. Guiver, H.B. Park, Polyamide thin-film composite membranes based on carboxylated polysulfone microporous support membranes for forward osmosis, *J. Membr. Sci.* 445 (2013) 220–227.
- [18] G.T. Gray, J.R. McCutcheon, M. Elimelech, Internal concentration polarization in forward osmosis: Role of membrane orientation, *Desalination* 197 (2006) 1–8.
- [19] Y. Gao, Y.N. Wang, W. Li, C.Y. Tang, Characterization of internal and external concentration polarizations during forward osmosis processes, *Desalination* 338 (2014) 65–73.
- [20] A. Saraf, K. Johnson, M.L. Lind, Poly(vinyl) alcohol coating of the support layer of reverse osmosis membranes to enhance performance in forward osmosis, *Desalination* 333 (2014) 1–9.
- [21] N. Navid, J. Mohsen, R. Ahmad, The effect of SiO₂ nanoparticles on morphology and performance of thin film composite membranes for forward osmosis application, *Desalination* 343 (2014) 140–146.
- [22] J. Su, T.S. Chung, Sublayer structure and reflection coefficient and their effects on concentration polarization and membrane performance in FO processes, *J. Membr. Sci.* 376 (2011) 214–224.
- [23] K.C. Khulbe, C. Feng, T. Matsuura, The art of surface modification of synthetic polymeric membranes, *J. Appl. Polym. Sci.* 115 (2010) 855–895.
- [24] C.S. Zhao, J.M. Xue, F. Ran, S.D. Sun, Modification of polyethersulfone membranes—A review of methods, *Prog. Mater. Sci.* 58 (2013) 76–150.
- [25] R. Malaisamy, R. Mahendran, D. Mohan, M. Rajendran, V. Mohan, Cellulose acetate and sulfonated polysulfone blend ultrafiltration membranes. I. Preparation and characterization, *J. Appl. Polym. Sci.* 86 (2002) 1749–1761.
- [26] D.L. Arockiasamy, A. Nagendran, K.H. Shobana, D. Mohan, Preparation and characterization of cellulose acetate/aminated polysulfone blend ultrafiltration membranes and their application studies, *Sep. Sci. Technol.* 44 (2009) 398–421.
- [27] X.K. Ma, N.H. Lee, H.J. Oh, J.S. Hwang, S.J. Kim, Preparation and characterization of silica/polyamide-imide nanocomposite thin films, *Nanoscale Res. Lett.* 5 (2010) 1846–1851.
- [28] D. Emadzadeh, W.J. Lau, A.F. Ismail, Synthesis of thin film nanocomposite forward osmosis membrane with enhancement in water flux without sacrificing salt rejection, *Desalination* 330 (2013) 90–99.
- [29] M. Pakizeh, A.N. Moghadam, M.R. Omidkhan, M. Namvar-Mahboub, Preparation and characterization of dimethyldichlorosilane modified SiO₂/PSf nanocomposite membrane, *Korean J. Chem. Eng.* 30 (2013) 751–760.
- [30] L. Yu, Z. Xu, H. Shen, H. Yang, Preparation and characterization of PVDF–SiO₂ composite hollow fiber UF membrane by sol–gel method, *J. Membr. Sci.* 337 (2009) 257–265.

- [31] A.L. Ahmad, M.A. Majid, B.S. Ooi, Functionalized PSf/SiO₂ nanocomposite membrane for oil-in-water emulsion separation, *Desalination* 268 (2011) 266–269.
- [32] A. Tiraferri, N.Y. Yip, W.A. Phillip, J.D. Schiffman, M. Elimelech, Relating performance of thin-film composite forward osmosis membranes to support layer formation and structure, *J. Membr. Sci.* 367 (2011) 340–352.
- [33] H. Li, Y. Lin, P. Yu, Y. Luo, L. Hou, FTIR study of fatty acid fouling of reverse osmosis membranes: Effects of pH, ionic strength, calcium, magnesium and temperature, *Sep. Purif. Technol.* 77 (2011) 171–178.
- [34] A. Tiraferri, N.Y. Yip, A.P. Straub, S. Romero-Vargas Castrillon, M. Elimelech, A method for the simultaneous determination of transport and structural parameters of forward osmosis membranes, *J. Membr. Sci.* 444 (2013) 523–538.
- [35] T. Li, P. Yu, Y. Luo, Preparation and properties of hydrophobic poly(vinylidene fluoride)-SiO₂ mixed matrix membranes for dissolved oxygen removal from water, *J. Appl. Polym. Sci.* 131 (2014) 4525–4529.
- [36] G.M. Geise, H.B. Park, A.C. Sagle, B.D. Freeman, J.E. McGrath, Water permeability and water/salt selectivity tradeoff in polymers for desalination, *J. Membr. Sci.* 369 (2011) 130–138.
- [37] C.Y. Tang, Q. She, W.C.L. Lay, R. Wang, Coupled effects of internal concentration polarization and fouling on flux behavior of forward osmosis membranes during humic acid filtration, *J. Membr. Sci.* 354 (2010) 123–133.